SLAC-PUB-95-7020

Compensation of Longitudinal Nonlinearities in the NLC Bunch Compressor[1]

F. Zimmermann and T. O. Raubenheimer

Stanford Linear Accelerator Center, Stanford University, Stanford, California 94309

The X-Band linac of the Next Linear Collider (NLC) will accelerate bunches of about 100 μm rms length to energies of 250–750 GeV. The task of the NLC bunch compressor is to reduce the initial bunch length of 4–5 mm, at extraction from the damping ring, by a factor of 40, to the desired value. This task is accomplished in two separate stages. The first stage at 2 GeV consists of an rf section and a wiggler. The second stage at 10 GeV is formed by an arc, an rf section, and a chicane. The system is designed such that the final bunch phase is insensitive to initial phase errors and to beam-loading in the intermediate S-band pre-linac. Additional decelerating rf sections are employed to compensate significant longitudinal aberrations.

INTRODUCTION

The design of the Next Linear Collider (NLC) calls for short bunches of about 10^{10} particles to be accelerated in an X-Band linac to energies of 250–750 GeV, at which point they are collided (1). A short bunch length is required in order to control the emittance growth caused by transverse wake fields in the X-Band linac and to avoid the luminosity reduction due to the 'hourglass effect' at the IP. The purpose of the NLC bunch compressor is to reduce the rms bunch length of about 4 mm at extraction from the damping rings to a value of 100 μm, which is suitable for injection into the main X-band linac and is equal to the vertical beta function at the IP.

In addition, to simply compressing the bunch length, there are a number of other requirements on the compressor. One of the most difficult is that the bunch compressor will have to compensate bunch-to-bunch phase errors due to beam-loading in the damping ring. This requires a net rotation of $\pi/2$ or $3\pi/2$ in the longitudinal phase space so that the phase errors are converted into energy errors. Similarly, the compressor also must compensate for beam loading effects originating in its various accelerating sections. Finally, the compressor should provide a trombone-like arm, reversing the direction of the

[1]Work supported by the Department of Energy, contract DE-AC03-76SF00515.

Work supported by Department of Energy contract DE–AC03–76SF00515.

beam before injection into the main linac. This gives space for abort systems, allows feed-forward from the ring to the linac, and facilitates future upgrades.

The proposed bunch compressor comprises two stages and an intermediate S-band pre-linac which accelerates the beam from 2 GeV to 10 GeV (2,3). Furthermore, the bunch compressor includes a spin rotator system and it provides tuning elements and diagnostics to correct dispersion and coupling. The design is illustrated in Figure 1.

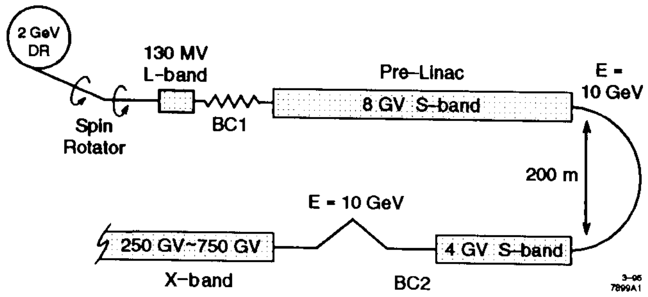

FIG. 1. Schematic of the NLC bunch compressor.

The parameters of the compressor system are chosen such that, first, the energy spread at the end of the X-band linac is smaller than the bandwidth of the final focus system, second, no significant energy tails are generated, and third, both the mean energy and the energy spread at the end of the linac are insensitive to the phase and energy errors resulting from beam loading in damping rings and pre-linac, respectively.

The phase error at extraction from the damping ring may be as large as $\pm 20°$ S-band (or ± 6 mm), while at the end of the pre-linac the energy variation over the bunch train due to multi-bunch beam loading is about 0.15% (4). The tolerance on the phase at the exit of the second compressor is $|\Delta z| <$10–20 μm in order to limit the relative energy change at the end of the main linac to 0.1%.

The following section describes the design of the two compressor stages. The origin of longitudinal nonlinearities and their impact on the performance are discussed in Section II. Section III presents a compensation scheme based on additional rf sections. Section IV describes the final beam distribution according to simulations. Some conclusions are drawn in Section V.

I. LAYOUT

The first compressor stage (BC1), at 2 GeV, consists of an rf and a wiggler section. It rotates the beam by 90 degree in the longitudinal phase space, such as to convert initial phase errors due to beam loading in the damping ring into energy errors, and reduces the bunch length by roughly a factor of 10, from about 4 mm to 500 μm. This is realized by an rf section which generates a δ-z correlation, followed by a bending section with energy-dependent path length. In this case, the bending section is a wiggler consisting of four 90° cells with quadrupoles at zero dispersion points (2). For a given rf frequency (here L-band), all other parameters are determined by the incoming beam. If the initial energy spread is $\delta \approx 10^{-3}$ the desired bunch length is obtained with $R_{56} = 0.5$ m. Parameters are listed in Table I; in the table, the superscript c refers to the compensating rf system discussed in the next section.

After BC1, a 500 m long S-band pre-linac accelerates the beam to 10 GeV. Following the pre-linac, the second compressor stage (BC2) performs a 360 degree rotation in phase space, and reduces the bunch length to 100 μm, appropriate for injection into the main X-band linac. A 360 (or 180) degree rotation is required to prevent bunch-to-bunch energy errors, caused by beam loading in the pre-linac or phase errors in the damping ring, from translating (back) into phase errors in the main linac.

The second compressor consists of an arc, a second S-band rf section and a chicane. In this case, two parameters may be selected independently, for instance, the rf frequency and the R_{56} of the chicane. We have chosen to use S-band rf because the waveform is more linear and transverse wakefields are much less severe than for X-band. The disadvantage of S-band is the additional length required; assuming similar gradients, one needs four times more S-band than X-band.

To reduce the nonlinearities in the longitudinal transformation (T_{566} term in TRANSPORT notation (5)) the R_{56} of the chicane is rather small, namely 36 mm. The necessary rf voltage is then 3.87 GV and the length of the accelerating section is large: 200 m. The arc comprises 80 FODO cells using separated function magnets and it does not include distributed sextupoles, the alignment tolerances for which would be severe. Its R_{56} (and thus the final bunch length) can be easily adjusted with the horizontal phase advance; see Fig. 2. The chicane is constructed from four 10 m bending sections (2). Additional parameters are given in Table I. Where two values are listed in the table, the first refers to the arc, the second to the chicane.

II. LONGITUDINAL NONLINEARITIES

The parameters are chosen as described, and thus the system has the desired linear transfer matrix for the longitudinal phase space. Unfortunately, tracking simulations still show a large variation of rms-energy-spread and mean energy at the end of the main linac as a function of initial phase error. For instance, a ± 6 mm initial phase error changes the final beam energy by roughly 0.2%–0.3% and the FWHM of the energy spread varies between 0.3% and 0.8%; these variations are too large to be tolerable.

The most important aberration of the system is the quadratic dependence of the final longitudinal phase on the incoming energy (the so-called T_{566} transfer-matrix element in TRANSPORT notation (5)) for the different subsystems.

To estimate its magnitude, let the trajectory of an arbitrary particle be

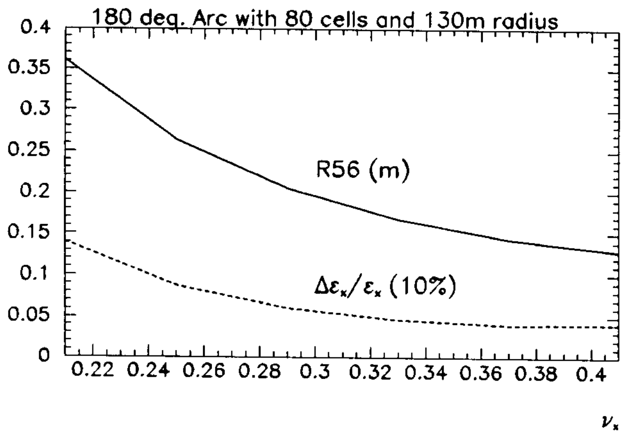

FIG. 2. R_{56} of the compressor arc and emittance growth due to synchrotron radiation in the arc as a function of horizontal phase advance per cell (in units of 2π).

described by a general dispersion function η as $x = \eta\delta$, where δ is the relative momentum deviation. The dispersion function may be expanded as a power series in δ:

$$\eta\delta = \eta_0\delta + \eta_2\delta^2 + \ldots \tag{1}$$

For a system of bending magnets and quadrupoles with bending radius ρ and gradient k, the functions η_0 and η_1 fulfill the differential equations (6)

$$\eta_0'' + \left(\frac{1}{\rho^2} + k\right)\eta_0 = \frac{1}{\rho} \tag{2}$$

$$\eta_1'' + \left(\frac{1}{\rho^2} + k\right)\eta_1 \approx -\frac{1}{\rho} + \left(k + \frac{2}{\rho^2}\right)\eta_0 \tag{3}$$

which, for $\eta_0 \ll \rho$, may be further approximated by

$$\eta_0'' + k\eta_0 \approx \frac{1}{\rho} \tag{4}$$

$$\eta_1'' + k\eta_1 \approx -\frac{1}{\rho} + k\eta_0 \tag{5}$$

The R_{56}- and T_{566}-matrix-elements may be expressed in terms of $\eta_{0,1}$ as

$$R_{56} = -\int \frac{\eta_0}{\rho} ds \tag{6}$$

$$T_{566} \approx -\int \left(\frac{\eta_1}{\rho} + \frac{1}{2}\eta_0'^2\right) ds \tag{7}$$

TABLE 1. Parameters of the two compressor stages. The R_{56} of the arc, together with the rf voltages V_{rf} and V_{rf}^c of BC2, is adjustable, which facilitates bunch-length changes by a factor of 2; see also Fig. 2.

	1st stage (BC1)	2nd stage (BC2)
Energy	2 GeV	10 GeV
σ_z	4 mm $\rightarrow$ 500 μm	500 μm $\rightarrow$ 100 μm
σ_e	0.1% $\rightarrow$ 1.0%	0.25% $\rightarrow$1.5%
V_{rf}	136 MV	3.85 GV
f_{rf}	1.4 GHz	2.8 GHz
L_{rf}	9 m	200 m
R_{56}	0.5 m	-21.1 cm, 36 mm
'R_{56}' length	100 m	370 m, 210 m
V_{rf}^c	6.9 MV	274 MV
f_{rf}^c	2.8 GHz	11.4 GHz
L_{rf}^c	0.5 m	8 m
total length	110 m	750 m

In case of wiggler and chicane $k\eta_{0,1} = 0$ and, therefore, $\eta_1 = -\eta_0$. Since $\eta_0'' \approx 1/\rho$, the second term in the expression for T_{566} can be integrated by parts, with the final result

$$T_{566} \approx -\frac{3}{2}R_{56} \qquad \text{(for wiggler and chicane)} \tag{8}$$

We note that, in order to reduce the T_{566}-matrix element, the value of the second order dispersion would have to be reduced. Unfortunately, this is difficult since changes to η_1 tend to adversely affect the transverse emittances.

For an arc, $k\eta_{0,1} \neq 0$ and there is no unique relation between R_{56} and T_{566}. In case of the bunch-compressor arc we find $T_{566} \approx 1.9 \cdot R_{56}$. Since energy variations and energy spread in the arc are quite small, its T_{566} is insignificant compared with the T_{566} coefficients of wiggler and chicane. It is the latter two which cause the large sensitivity of final energy to initial phase. The sensitivity arises as follows. Initial phase errors cause energy errors δ_1 after the first compressor rf, which in turn, due to the T_{566} of the wiggler, give rise to a phase offset in the pre-linac. The result is an additional energy change $\Delta\delta_{pl}$ which may either add to or cancel the energy error δ_1, depending on the sign of the offset. The second compressor further enhances the energy error and, due to the T_{566} of the chicane, generates a significant phase error in the main linac. A second effect, that is not very important for the NLC parameters, is that the T_{566} will cause the bunch to be asymmetric in z. This effect can be much more significant when compressing a greater amount.

III. COMPENSATION

Because the T_{566} in the wiggler and chicane severely degrade the performance of the compressor, we need to compensate for the effect. There are three possible approaches: (1) directly reduce the T_{566}, (2) compensate for the effect globally, or (3) compensate locally. As mentioned, the direct reduction is difficult. The simplest approach is to utilize sextupole magnets. Unfortunately, in the NLC, the beams are flat with an emittance ratio of 100:1. Thus, to prevent vertical emittance dilution due to skew coupling, the sextupoles have very tight vertical alignment tolerances. Alternately, one can try to modify the η_1 without changing the η_0 with the quadrupole lattice. Unfortunately, this breaks the simple symmetry of the wiggler and chicane systems and it becomes difficult to minimize the higher-order chromatic emittance dilutions.

The global compensation method relies upon choosing the parameters of the two compressors so that the second compressor cancels the effect of the T_{566} in the first compressor. While this is possible, and is similar to the first-order compensation scheme proposed for the LCLS bunch compressor (7), such a scheme is not satisfactory. Unfortunately, the global schemes are much more sensitive to the detailed parameters of the compressors and would inhibit the tuning flexibility during operations. Furthermore, the system would have to be re-tuned when changing bunch currents since the longitudinal wakefields are significant and must be considered.

For these reasons, we have adopted a local compensation technique where the compensation is performed with an additional decelerating rf, located in the compressor before the bending magnets of the wiggler of chicane. The purpose of this rf is to cancel the quadratic dependence of the final phase z_f on the longitudinal position (the phase error) at the compressor rf. Consider the main compressor rf

$$V \sin(-kz) \tag{9}$$

and a compensating rf

$$-V^c \cos(-k^c z) \tag{10}$$

with V^c small compared with the beam energy E, $V^c \ll E$, followed by a chicane or a wiggler. The phase z_f at the exit of this system depends on the initial phase z_{rf} at the rf as

$$z_f = (1 - R_{56} f) z_{rf} + T_{566} f^2 z_{rf}^2 + \frac{1}{2} R_{56} f^c k^c z_{rf}^2 \tag{11}$$

Here, f^c is the value of $V^c k^c / E$ for the compensating rf, and $f \equiv Vk/E$ the corresponding value for the main compressor rf; $k \equiv 2\pi/\lambda$ being the wave number. The sum of the quadratic terms in Eq. (11) is zero if we choose

$$V_c = -2 \frac{T_{566}}{R_{56}} \frac{k^2 V^2}{k^{c2} E} = 3 \frac{\lambda_c^2 V^2}{\lambda^2 E} \tag{12}$$

where we have used Eq. (8). The required voltage V^c is about 7 MV and 300 MV for an S-band and an X-band compensation in the first and second compressor stage, respectively.

TABLE 2. Four different NLC scenarios considered in the bunch-compressor simulations.

	NLC-Ia	NLC-Ic	NLC-IIa	NLC-IIc
rms bunch length	100 μm	150 μm	125 μm	150 μm
N/bunch [10^{10}]	0.65	0.85	0.95	1.25
$E_{\max}$ [GeV]	267	233	534	473

The residual longitudinal aberrations are now of third and higher order. An initial phase error or multi-bunch beam loading may cause an energy offset of the entire bunch at the entrance to BC2. In addition, the longitudinal wakefields in the pre-linac induce a (mainly) quadratic δ-z-correlation, where z is the longitudinal position of a single particle with respect to the bunch center, and δ the relative momentum deviation of a single particle at the end of the pre-linac. Due to the R_{56} of the arc, this energy error translates into a position error at the two rf systems of BC2, which is transformed once more into energy by the rf, and back into longitudinal phase by the T_{566} of the chicane. The final phase z_f of a single particle at the exit of BC2 is

$$z_f \approx az - bz^4 - c\delta^2 z^2 - d\delta z^2 - e\delta z^4 + \ldots \tag{13}$$

where $a \approx 1/5$–$1/7$ is the desired linear compression ratio, and the four non-linear terms on the right-hand side are about the same size (10–20 μm), for typical values $\delta \approx \pm 0.004$ and $z \approx 500$ μm. These four terms would be negligibly small if the pre-linac wakefields were absent.

IV. PERFORMANCE

To determine the optimum parameters of the system, we have considered four NLC scenarios, corresponding to different bunch lengths and energies (see Table IV). In all scenarios, computer simulations of the longitudinal single-bunch dynamics have been performed using a modified version of the code LITRACK (8). In these simulations a distribution of particles, as extracted from the damping ring, is tracked through the different compressor subsystems and the main X-band linac.

In the simulation, studies the phase of the X-band linac was adjusted to obtain a final full-width-half-maximum energy spread of about 0.8%. This energy spread is slightly smaller than the energy bandwidth of the final focus. Figures 3–5 illustrate tracking results for NLC-Ia (Table IV). The figures show the longitudinal and energy profiles at the end of the main linac for three different injection phases, $\Delta z = 0, +6$ mm, -6 mm, demonstrating the insensitivity of the final beam distribution to initial phase errors.

In Figure 6, the average energy is plotted as a function of the initial phase, for four different NLC scenarios (Table 2). Figures 7 and 8 show equivalent pictures for the rms and full-width-half-maximum energy spread, respectively. These figures illustrate that average energy and energy spread at the end of the main linac vary by no more than 0.1% for initial phase errors up to $\pm 20°$ S-band (or ± 6 mm).

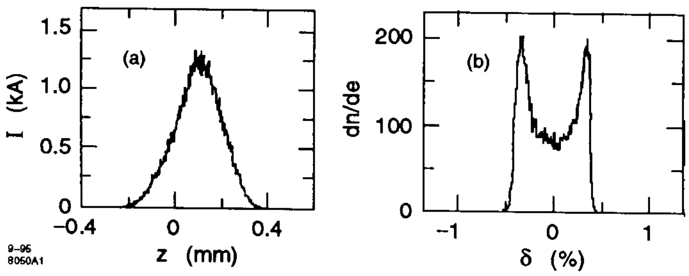

FIG. 3. Longitudinal position and energy profiles at the end of the NLC main linac for $N_e = 6.5 \times 10^9$ particles per bunch and a final bunch length of 100 μm (NLC-Ia); the initial phase error was zero.

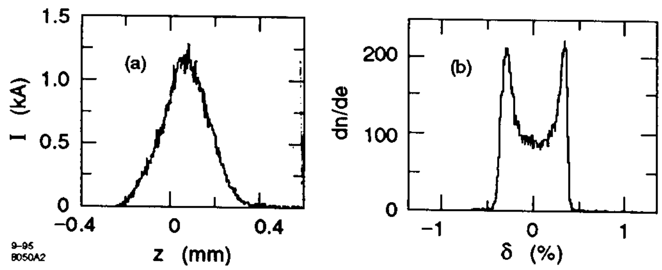

FIG. 4. Longitudinal position and energy profile at the end of the NLC main linac for $N_e = 6.5 \times 10^9$ particles per bunch and a final bunch length of 100 μm (NLC-Ia); the initial phase error was +6 mm. injection phase error.

V. CONCLUSION

A design of a two-stage bunch compressor for the NLC has been described. To minimize the impact of nonlinearities in the longitudinal phase space, the compressor parameters had to be carefully chosen, and, specifically, large compressor voltages were required. In addition, it proved necessary to compensate the dominant longitudinal aberration. We use a local compensation which is provided with dedicated rf sections. The performance of the final scheme surpasses the design goals.

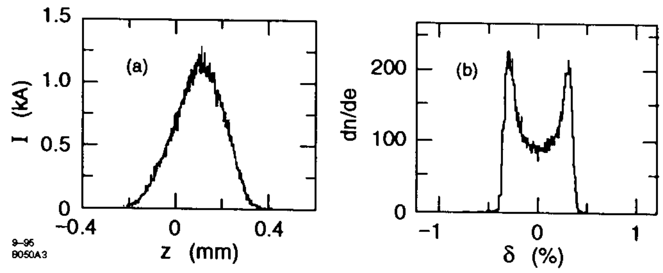

FIG. 5. Longitudinal position and energy profile at the end of the NLC main linac for $N_e = 6.5 \times 10^9$ particles per bunch and a final bunch length of $100\,\mu$m (NLC-Ia); the initial phase error was -6 mm.

REFERENCES

1. T. Raubenheimer et al., "Parameters of the SLAC Next Linear Collider", Proc. of 1995 Part. Acc. Conf., Dallas, (1995); and SLAC–PUB–6849 (1995).
2. T. Raubenheimer, P. Emma, S. Kheifets, "Chicane and Wiggler Based Bunch Compressors for Future Linear Colliders," Proc. of 1993 Part. Acc. Conf., Washington (1993) 635; T. Raubenheimer, *NLC Note* **2** (1994).
3. P. Emma, T. O. Raubenheimer, F. Zimmermann, "A Bunch Compressor for the Next Linear Collider", Proc. of 1995 Part. Acc. Conf., Dallas, (1995); and SLAC–PUB–6787 (1995).
4. R. Miller, private communication (1994).
5. K. Brown, F. Rothacker, D. Carey, C. Iselin, "TRANSPORT - A Computer Program for Designing Charged Particle Beam Transport Systems", *SLAC*-**91** (1977).
6. J.P. Delahaye and J. Jäger, "Variation of the Dispersion Function, Momentum Compaction Factor and Damping Partition Numbers with Particle Energy Deviation", *Part. Acc.* **18** 183 (1985).
7. K.L. Bane, T.O. Raubenheimer, J.T. Seeman, "Electron Transport of a Linac Coherent Light Source (LCLS) using SLAC Linac," Proc. of 1993 Part. Acc. Conf., Washington (1993) 596.
8. The program LITRACK for simulating longitudinal wakefield effects in linear accelerators was written by K. Bane.

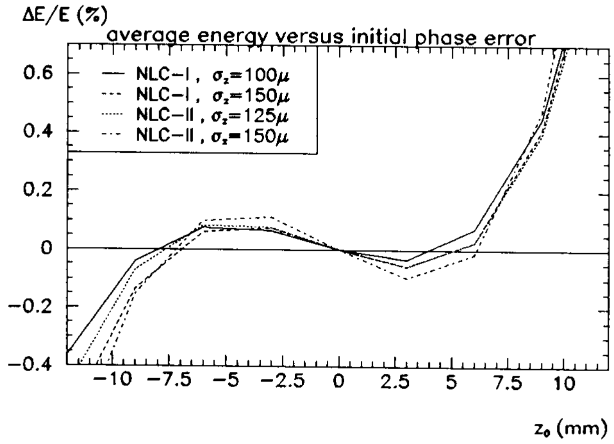

FIG. 6. Variation of the average beam energy at the end of the NLC main linac with the initial phase error for the cases: NLC-Ia, NLC-Ic, NLC-IIa, and NLC-IIc; the nominal beam energy is roughly 250 GeV in NLC-I and 500 GeV in NLC-II.

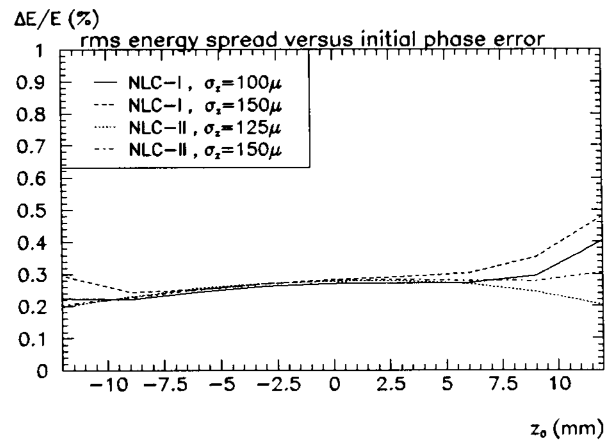

FIG. 7. Variation of the rms energy spread at the end of the NLC main linac with the initial phase error, for the cases: NLC-Ia, NLC-Ic, NLC-IIa, and NLC-IIc.

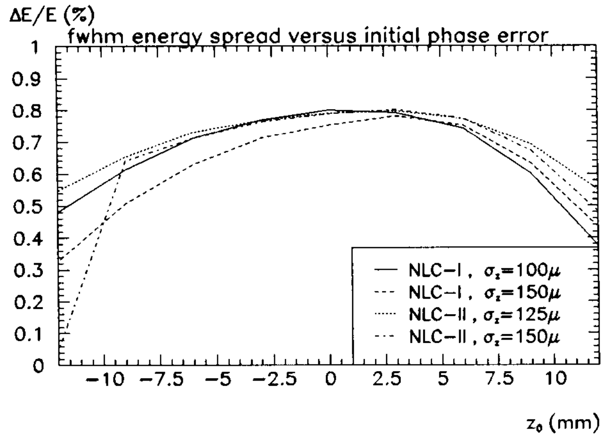

FIG. 8. Variation of the FWHM energy spread at the end of the NLC main linac with the initial phase error for the cases: NLC-Ia, NLC-Ic, NLC-IIa, and NLC-IIc.